MODELING of 5-AXIS MILLING FORCES and FORM ERRORS

by

ERDEM ÖZTÜRK

Submitted to the Graduate School of Engineering and Natural Sciences
in partial fulfillment of
the requirements for the degree of
Master of Science
in

SABANCI UNIVERSITY

Spring 2005

Abstract

5-axis milling operations are common in several industries such as aerospace, automotive and die/mold for machining of sculptured surfaces. In almost all of these operations, the dimensional tolerance integrity and surface quality are of utmost importance. Part and tool deflections under cutting forces may result in unacceptable part quality. Process models can be used to determine the proper or optimal milling conditions for required quality with higher productivity. Majority of the milling models have been developed for 3-axis operations, even the ones for ball-end mills. In this thesis, a complete kinematics and force model is presented for 5-axis milling operations using ball-end mills. The effects of lead and tilt angles are included in the model, and presented in the thesis. Tool deflections due to the cutting forces are also formulated for 5-axis milling. Model predictions for cutting forces are compared and verified by experimental results.

Özet

5 eksen freze operasyonları havacılık, otomotiv ve kalıpçılık sektörlerinde karmaşık yüzeylerin talaşlı imalatında sıklıkla kullanılır. Bütün bu operasyonlarda boyut toleransları ve yüzey kalitesi çok önemlidir. Parçada veya kesici takımda kesme kuvvetleri nedeniyle oluşan deformasyonlar kabul edilemeyecek parça kalitesine sebep olabilirler. İstenilen kalitenin daha yüksek bir verimlilik ile sağlanması için gerekli olan en iyi frezeleme koşulları süreç modelleri kullanılarak bulunabilir. Küresel uçlu freze takımı için geliştirilenler de dahil olmak üzere, freze modellerinin çoğu 3 eksen operasyonlar için geliştirildi. Bu tezde, küresel uçlu takım kullanılan 5 eksen freze operasyonlari için geliştirilen bir kuvvet modeli sunuldu. Lead ve tilt açılarının etkileri modele dahildir. 5 eksen frezeleme için, kesme kuvvetlerinden dolayı oluşan kesici takım üzerindeki deformasyonlar formüle edildi. Kesme kuvvetleri için modelin tahminleri deneysel sonuçlarla karşılaştırıldı ve doğrulandı.

Table of Contents

List of Tables

List of Figures

Acknowledgement

I would like to express my sincere appreciation to my research supervisor Dr. Erhan Budak for his perpetual guidance, support and encouragement throughout my graduate studies at the Sabanci University.

I am grateful to my colleagues in the Industrial Automation Laboratory. They have shared their knowledge, experience with me, which have made my life at Sabanci University easier and more enjoyable. I would like to thank Mehmet Güler, Emre Özlü, Lütfi Taner Tunç, and Evren Bal for their friendship and endless support. My special thanks are to my love, Neşe Tüfekçiler, for being the joy of my life.

Finally, I am deeply grateful to my beloved parents, Vural and Pakize Öztürk; my dear brother; Özcan for their constant support, patience and encouragement during my graduate study. I dedicate this work to my family.

Chapter 1
Introduction

5-axis ball-end milling is an important process for aerospace, automotive and die/mold industries. It is used extensively in manufacturing of free form surfaces such as dies and molds, turbine engine and aircraft structural components. In many cases the manufacturing tolerances are very tight due to the required high quality and dimensional surface integrity. Tool and part deflections are major contributors to the dimensional errors. They can be predicted and kept under control by modeling the 5-axis milling forces.

In 5-axis milling, there are two more cutting parameters in addition to the 3 axis milling. The first one is the lead angle, angular rotation of the cutting tool about the direction perpendicular to the feed direction, and the second one is the tilt angle, angular rotation of the tool about the feed direction. These angles can be positive, zero and negative. If the 3 axis milling case is excluded in which lead and tilt angles are zero, there are 8 different cutting modes in 5-axis milling (Figure 1-1). For a given cutting process, selecting the optimum cutting mode and corresponding optimum lead and tilt angle values are challenging. Modeling of 5-axis milling forces and form errors can turn these challenges to an opportunity.

In industry, generally lead and tilt angles are selected based on experience or by trial and error. Hence, the 5-axis milling model presented in this thesis will be significantly beneficial for the industry.

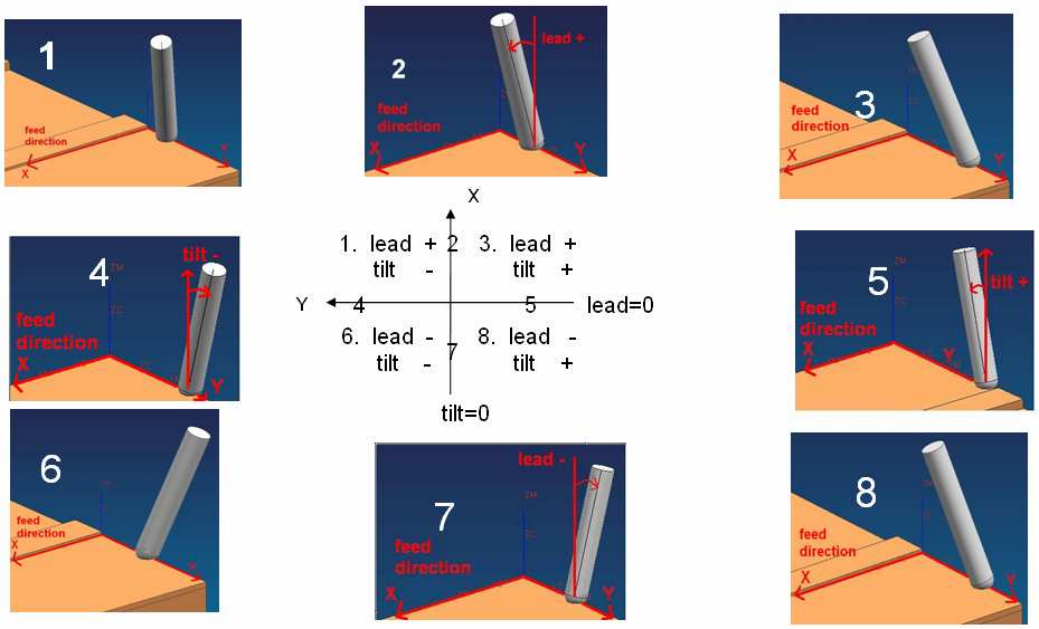

Figure 1-1.Cutting modes in 5-axis Milling

1.1 Research Objective

The thesis has the following objectives:

- To be able to predict cutting forces in 5-axis milling operations
- To model the tool deformation under cutting forces
- To find the optimum combination of cutting parameters for a 5-axis milling operation

1.2 Organization of the Thesis

The thesis is organized as follows: The review of related literature is presented in Chapter 2, followed by the geometry of ball-end mill in Chapter 3. Cutting edges of the ball-end mill are divided into oblique cutting elements with varying geometry according to its location on the cutting edge. Geometry of ball-end mill is modeled considering the local helix, lag angle and local uncut chip thickness. Then engagement boundaries are defined in 3-axis ball-end milling. Unlike flat end milling, start and exit angles are not constant for a given cutting process in ball-end milling, they are function of the axial position on the ball-end mill. In Chapter 4, 5-axis milling geometry is presented. Effect of lead and tilt angles on ball-end mill geometry, engagement boundaries and uncut chip thickness is expressed. Force model is presented in Chapter 5, followed by optimum lead and tilt angle predictions in Chapter 6. Form error formulation is given in Chapter 7 where predicted cutting forces are used in the modeling of tool deflections. In Chapter 8, simulation and experiment results are presented. Thesis is concluded with the summary of contributions in Chapter 9.

Chapter 2
Literature Review

Due to the need for higher quality in machining industry, force and form error analysis have become a major consideration in high precision applications. In the past years, many researchers have done significant amount of work in modeling of 3-axis ball-end milling. However, in only a few of these studies 5-axis milling has been considered. An overview of the major relevant published works is given in the chapter.

2.1 Force Model

Metal cutting mechanics can be analyzed by orthogonal and oblique models. However, nearly all practical cutting processes are oblique. Mechanics of oblique cutting has been investigated in several works, two important ones being by Armarego [1] and Merchant [2]. Although the formulation of the process mechanics in many of the studies is similar, there are significant differences in the approach used in implementing the models for force prediction of practical processes. The main difficulty in machining process modeling is obtaining the material data, and this is where the approaches vary from completely analytical to completely experimental.

One analytical approach is to use the flow stress and thermal properties of the workpiece material in the analysis. Shatla, et al. [3] divided ball-end mill into oblique cutting elements that have geometries and cutting conditions that vary with the location of the element on the cutting edge. Using flow stress relation and the thermal characteristics of Ti_6Al_4V alloy [4,5] for each element, they predicted ball-end milling forces. Another analytical approach is so called, thermomechanical modeling. In this approach, the work material is described by a material model such as the Johnson–Cook law. The material characteristics such as strain rate sensitivity, strain hardening and thermal softening are

considered. This is the approach used by Moufki, et al. [6] where a thermomechanical model was employed for the oblique cutting process.

In the mechanistic approach, edge and cutting force coefficients are calibrated for different workpiece and cutting tool material pairs through milling tests which has also been used for ball-end milling. Gradisek et al. [7] presented a procedure for identification of specific cutting and edge force coefficients from milling tests with an arbitrary radial immersion for a variety of end mill shapes, such as cylindrical, taper, ball and bull nose, etc.

Yucesan, et al. [8] and Lazoglu [9] are among the authors who modeled 3-axis ball-end milling using the mechanistic approach. Yucesan's model is based on the analytic representation of ball shaped helical flute geometry, and its rake and clearance surfaces. The pressure and friction coefficients are identified from a set of slot ball-end milling tests at different feeds and axial depth of cuts, and are used to predict the cutting forces for various cutting conditions. Lazoglu presented a mechanistic force model that has the ability to calculate the workpiece/cutter intersection domain automatically for a given cutter location (CL) file. An analytical approach was used to determine instantaneous chip load and cutting forces considering run-out.

In the mechanics of milling approach, the cutting force coefficients are predicted using the oblique cutting model and the orthogonal cutting database. Budak, et al. [10] presented the method for orthogonal to oblique transformation. Shear stress, shear angle and friction angle are identified from orthogonal turning tests and they are inserted into oblique cutting model for calculating cutting force coefficients. Edge force coefficients are directly taken from orthogonal cutting tests. Mechanics of milling approach was employed by several authors for cutting force prediction in 3-axis ball-end milling. Lee, et al. [11] , Yang, et al. [12] , Sadeghi et al. [13] and Tai, et al. [14] are some of these authors. In these studies, engaged cutting edge is divided into differential oblique elements. Corresponding orthogonal database is transformed to these differential oblique elements and differential cutting forces are calculated. For each tool rotational position, the cutting forces are found by summing the differential cutting forces.

Although there have been several works on the modeling of 3-axis ball-end milling processes, this has been very limited for 5-axis operations. The work of Lazoglu and Liang [15] on modeling of ball-end milling with cutter axis inclination was a bridge between modeling of 3-axis and 5-axis milling operations. Lazoglu represented the effect of inclination angle on the cutter-workpiece engagement domain. In one of the important works on ball-end milling, Lee and Altintas [11] modeled 3-axis ball-end milling using orthogonal to oblique transformation. Geometric modeling of 3-axis milling in this thesis is mostly based on their work. Fussel, et al. [16] used discrete geometric models of tool and an extended Z-buffer model of the workpiece to determine the tool-workpiece contact area. Similarly, Clayton, et al. [17] discretized the tool and workpiece in order to find the contact area. Zhu, et al. [18] modeled the cutting edge profile in analytical form and determined the engaged cut geometry by classification of the cutting point positions with respect to the workpiece surface. In all these studies, mechanistic model was applied to estimate the cutting forces acting on the tool for 5-axis force modeling.

In this thesis, cutting forces in 5-axis ball-end milling are modeled by using mechanics of milling approach, i.e. orthogonal to oblique transformation. This method needs orthogonal cutting data for a given work material. However, once this data is obtained, it can be applied to any cutter geometry, unlike mechanistic approach where the force coefficients have to be calibrated for each material and cutting tool pair.

2.2 Form Error Model

There are several works on the prediction of form errors due to the 3 axis ball-end milling. Budak, et al. [19] calculated form error for flat end milling by using both FEM and beam models. Moreover, they presented a method that will give the optimum feed and radial depth of cut values to keep the form error at a minimum. Kim, et al. [20] predicted cutting forces in 3-axis ball-end milling by determining the cutting engagement boundary using Z-map and created a form error model by modeling the cutting tool as a cantilever beam.

Similarly, Ryu, et al. [21] predicted form error in flat end milling by using the beam theory. Up to now, no work, that predicts form errors due to 5-axis ball-end milling, has been encountered in the literature. In that sense, this thesis is an original contribution to the literature.

2.3 Summary

In this chapter, an outline of the literature in metal cutting mechanics, force and form error models in 3-axis ball-end milling and force models in 5-axis ball-end milling has been presented.

Chapter 3
Geometry of Ball-End Mill

3.1 Introduction

Ball-end mills are mainly used in semi-finishing and finishing operations in 3-axis and 5-axis milling. In order to model 3 and 5-axis ball-end milling forces and form errors, geometry of the ball-end mill is presented in this chapter.

Figure 3-1 Ball-End Mill

3.2 Ball-End Mill Geometry

The detailed geometry of a ball-end mill is shown in Figure 3-2. A Cartesian coordinate system xyz is defined at ball tip. The z-axis is the axial direction of the cutter whereas x axis is collinear with the feed direction, y axis being normal to the both.

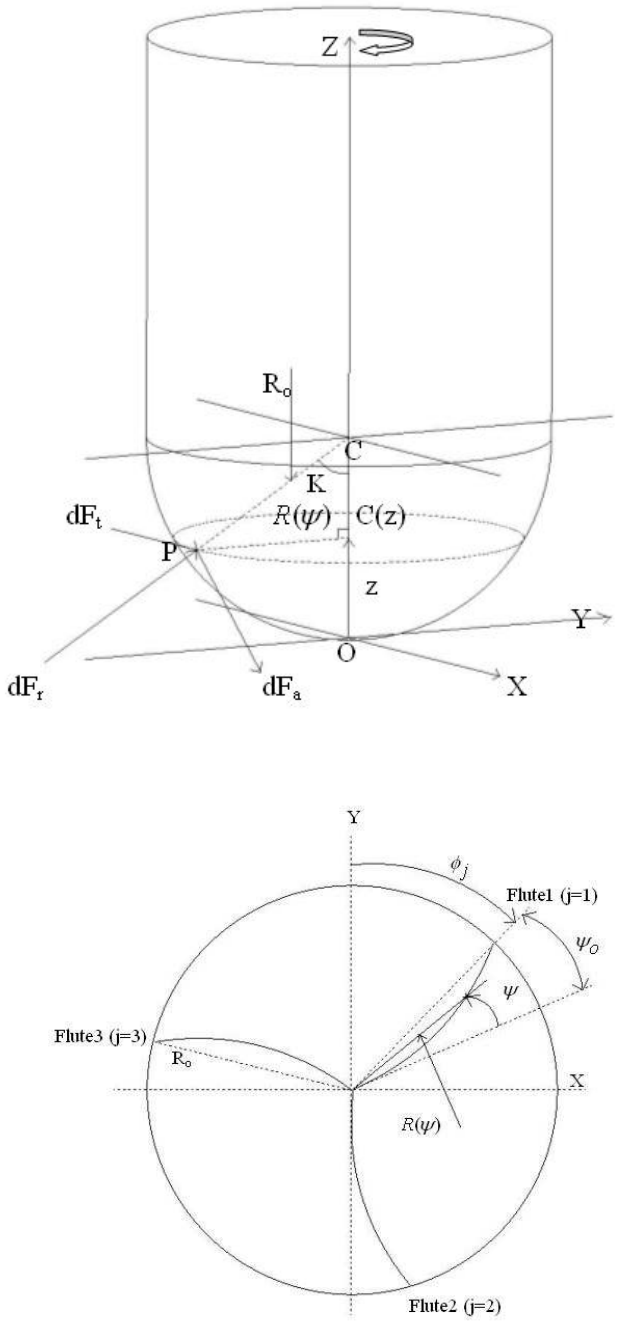

Figure 3-2 Geometry of ball-end mill

Axial location of a point on a cutting edge can be defined by three parameters: lag angle ψ, axial position z and angle K (Figure 3-2). They can be written in terms of each other as:

$$z = \frac{R(\psi)\psi}{\tan i(\psi)} = R_o(1-\cos K) \tag{3.1}$$

where $R(\psi)$ is local radius, $i(\psi)$ is the local helix angle and K angle is defined in Figure 3-2 and Figure 3-4.

For cutters which have constant lead length, at any two different points on a cutting edge, the following relation is valid.

$$\frac{z_1}{\psi_1} = \frac{z_2}{\psi_2} \tag{3.2}$$

So from Eq. (3.1) and Eq. (3.2)

$$\frac{R(\psi_1)}{\tan i(\psi_1)} = \frac{R(\psi_2)}{\tan i(\psi_2)} = \frac{R_o}{\tan i_o} \tag{3.3}$$

Rearranging the terms in Eq. (3.3), it is seen that local helix angle is scaled by a radius factor, and can be expressed in terms of i_o where i_o is the oblique angle at ball and shank meeting boundary (Figure 3-3):

$$\tan i(\psi) = \tan i_o \frac{R(\psi)}{R_o} \tag{3.4}$$

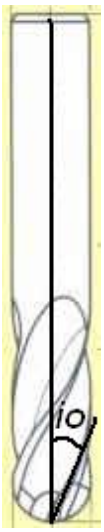

Figure 3-3 Helix angle i_o at the ball and shank meeting boundary

[Picture is from Kennametal Catalogue]

Eq. (3.1) now can be defined in such a way that only the variables are z and lag angle ψ :

$$z = \frac{R_o}{\tan i_o}\psi \tag{3.5}$$

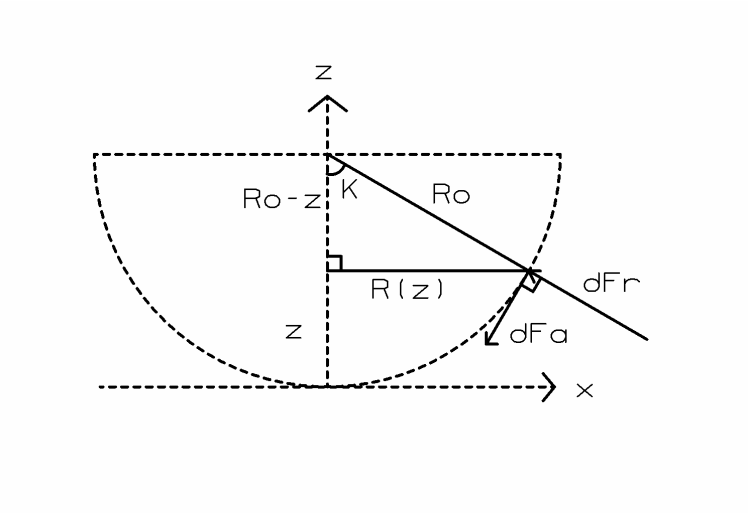

Figure 3-4 Local radius at a cross-section

The local radius of ball-end mill changes with the axial distance from ball tip. At z=0 (tool tip) local radius is zero, whereas it equals to R_o at z=R_o .By using the geometric relation in Figure 3-4, the local radius can be expressed in terms of z as:

$$R(z) = \sqrt{R_o{}^2 - (R_o - z)^2} \tag{3.6}$$

Using Eq. (3.5) and Eq. (3.6), the local radius can be expressed in terms of the lag angle as follows:

$$R(\psi) = R_o \sqrt{1 - (\psi \cot i_o - 1)^2} \tag{3.7}$$

A vector r is drawn from the ball center to a point P on the cutting edge in Figure 3-2:

$$\boldsymbol{r}(\psi) = \boldsymbol{OP} - \boldsymbol{OC} \tag{3.8}$$

$$\boldsymbol{OP} = \begin{bmatrix} R(\psi)\sin\phi_j \\ R(\psi)\cos\phi_j \\ R_o\psi\cot i_o \end{bmatrix} \tag{3.9}$$

$$\boldsymbol{OC} = R_o\boldsymbol{k} \tag{3.10}$$

From Eq. (3.8)-(3.10),

$$\boldsymbol{r}(\psi) = \begin{bmatrix} R(\psi)\sin\phi_j \\ R(\psi)\cos\phi_j \\ R_o(\psi\cot i_o - 1) \end{bmatrix} \tag{3.11}$$

The length of the infinitesimal curved cutting edge *dS* along the ball part is computed from

$$dS = \|dr\| = \sqrt{(R'(\psi)^2 + R^2(\psi) + {R_o}^2 \cot^2 i_o}\, d\psi \tag{3.12}$$

$R'(\psi)$ is the derivative of $R(\psi)$ with respect to ψ

$$R'(\psi) = \frac{-R_o(\psi \cot i_o - 1)\cot i_o}{\sqrt{1-(\psi \cot i_o - 1)^2}} \tag{3.13}$$

Immersion angle ϕ_j defines the angular orientation of a point on the cutting edge of a flute according to ball-end-mill's longitudinal axis, measured from +y direction as shown in Figure 3-2:

$$\phi_j = \phi_{ref} + (j-1)\phi_p - \frac{\tan i_o}{R_o} z = \phi_{ref} + (j-1)\phi_p - \psi$$

$$= \phi_{ref} + (j-1)\phi_p - \tan i_o (1 - \cos K) \tag{3.14}$$

where

$$\phi_p = \frac{2\pi}{n} \text{ and } K = \sin^{-1}(\frac{R(z)}{R_o}) = \sin^{-1}(\frac{R(\psi)}{R_o}) \text{ (from Figure 3-4)} \tag{3.15}$$

n denotes the teeth number on the ball-end mill and subscript j defines the corresponding tooth.

3.3 Uncut Chip Thickness

Uncut chip thickness depends on feed per tooth f_t, immersion angle ϕ_j and K angle and calculated by the equation below.

$$t(\phi_j, K) = f_t \sin\phi_j \sin K \tag{3.16}$$

Chip width *db*, shown in Figure 3-5, which is tangent to cutting edge:

$$db = \frac{dz}{\sin K} \tag{3.17}$$

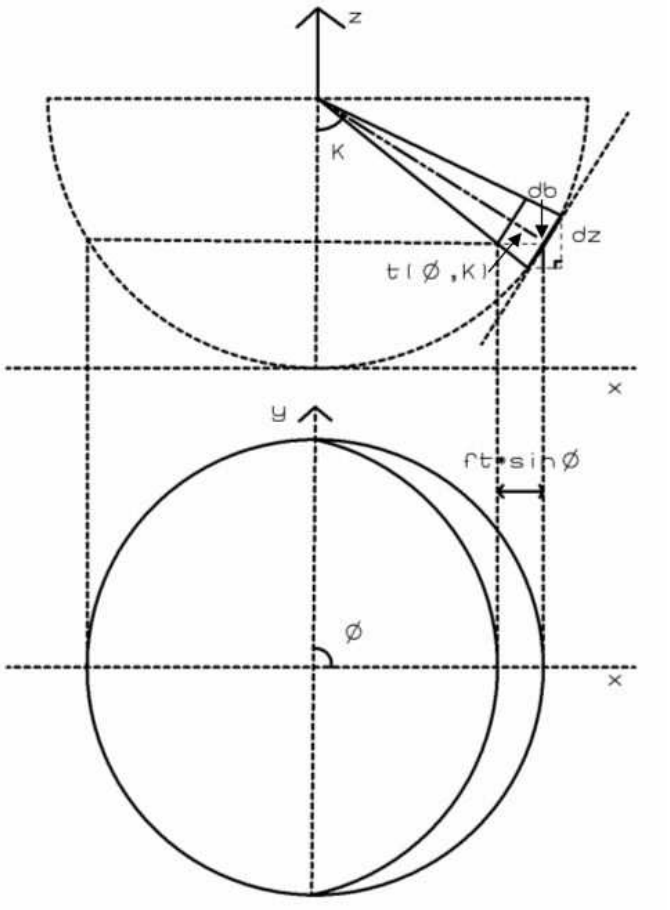

Figure 3-5 Geometric representation of differential cutting area

3.4 Engagement Boundaries in 3-axis milling

Since the radius of the ball-end mill is changing in z-direction, engagement boundaries, namely start and exit angles, are function of axial position z, unlike flat-end milling where start and exit angles are constant along the axial position of the cutter. Ball-end mill is divided into differential disc elements having height of *dz* and start, exit angles are determined for each element. The calculation of start and exit angles are explained below.

There are two different cases in engagement boundary calculation. In the first case, the tool cuts a non-machined cubic solid and in the second case it cuts a previously machined surface. Slot cutting, is the common point of these two cases. Start and exit angle calculations are given below for both of these cases.

3.4.1 The first case: Machining of a cubic solid

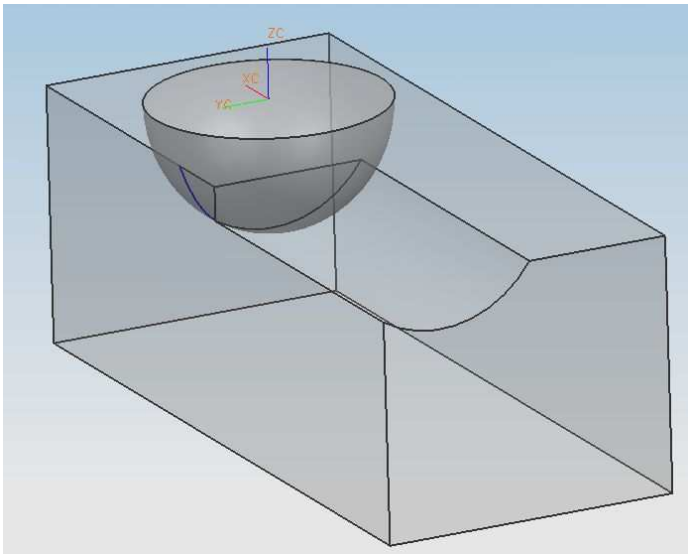

Figure 3-6 Machining of a cubic solid

In this case, in addition to the fact that the engagement boundaries vary in the axial direction, their definition also change after a critical point at a height of *hc* which depends on

the radial depth of cut *s,* the axial depth of cut *a* and the radius of the ball-end mill R_o. *hc* is shown in Figure 3-8 and can be obtained by the equation below.

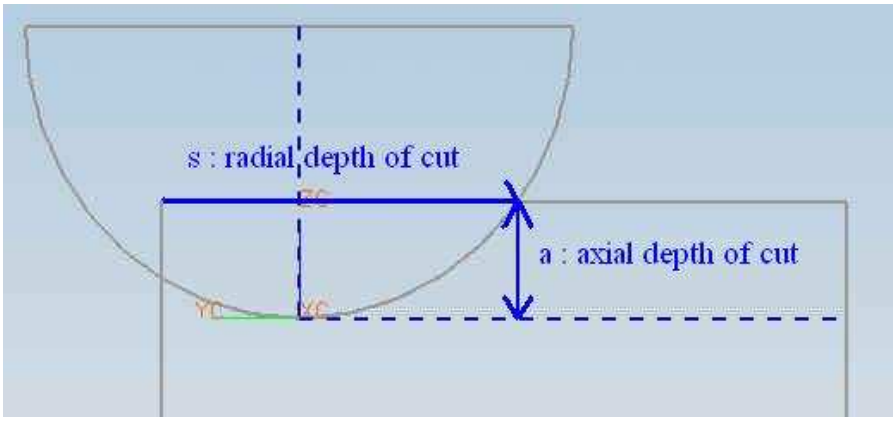

Figure 3-7 Illustration of *s* and *a*

$$hc = R_o - \sqrt{R_o{}^2 - (s - R(a))^2} \tag{3.18}$$

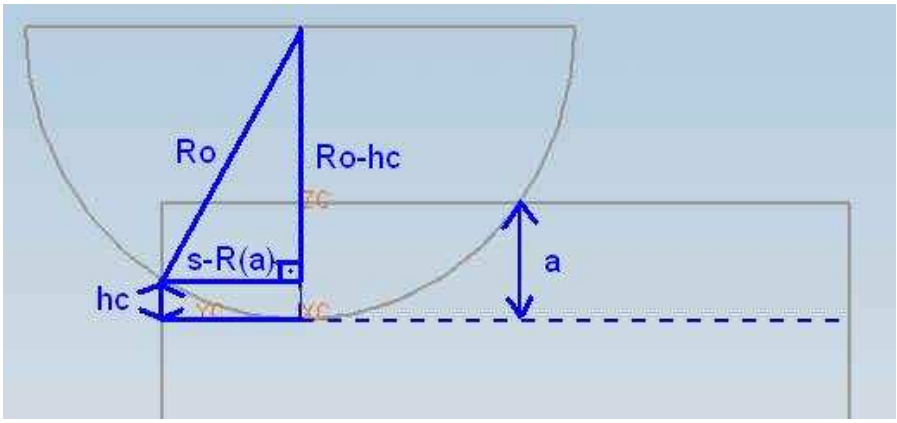

Figure 3-8 *hc* definition

R(a) is the radius of the ball-end mill at *z=a* and it can be calculated by the following equation (Figure 3-9):

$$R(a) = \sqrt{{R_o}^2 - (R_o - a)^2} \tag{3.19}$$

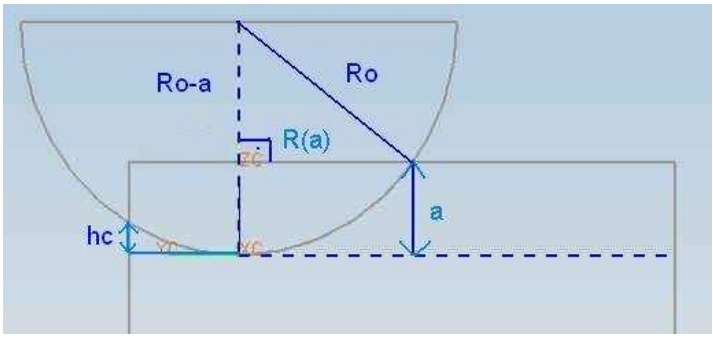

Figure 3-9 *R(a)* definition

Immersion boundaries calculation is different for down-milling and up-milling cases.

1. Down milling

In down milling exit angle is always π; start angle depends on axial, radial depth of cut and axial position *z* when the axial position *z* is above the *hc*. In this case:

$$\phi_{st}(z) = \pi - \cos^{-1}\left(\frac{R(a) - s}{R(z)}\right) \tag{3.20}$$

In the case when the axial position z is at a lower level than *hc*, there are 2 different situations according to the radial depth of cut value. If radial depth of cut is greater than *R(a)*, start angle is:

$$\phi_{st}(z) = 0 \tag{3.21}$$

If radial dept of cut *s* is less than *R(a)* (Figure 3-10), then there is no cutting below *hc* level and start angle is also π.

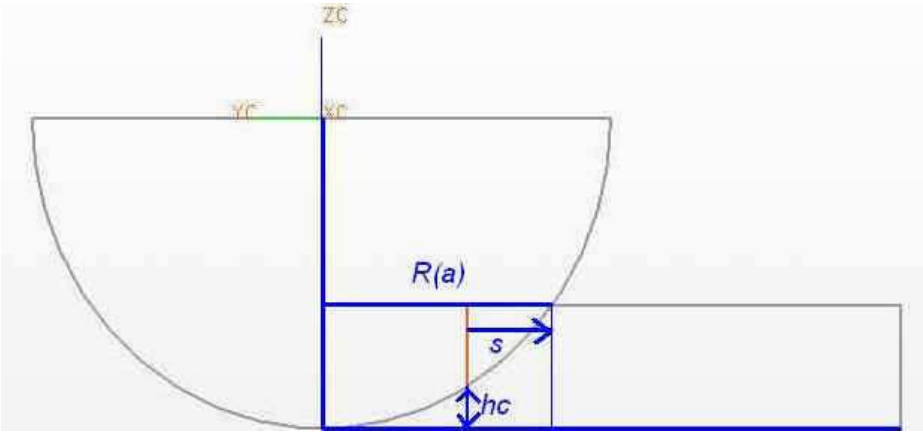

Figure 3-10 $s \leq R(a)$ case

2. Up milling:

In up milling start angle is always zero; exit angle depends on axial, radial depth of cut and axial position *z* when the axial position *z* is above the *hc*. In this case:

$$\phi_{ex}(z) = \cos^{-1}\left(\frac{R(a)-s}{R(z)}\right) \tag{3.22}$$

In the case when the axial position *z* is at a lower level than *hc,* there are 2 different situations according to the radial depth of cut value. If radial depth of cut is greater than *R(a)*, exit angle is:

$$\phi_{ex}(z) = \pi \tag{3.23}$$

If radial dept of cut is less than *R(a)*, then there is no cutting below *hc* level and exit angle is also zero.

3.4.2 The second case: Machining of a previously machined surface

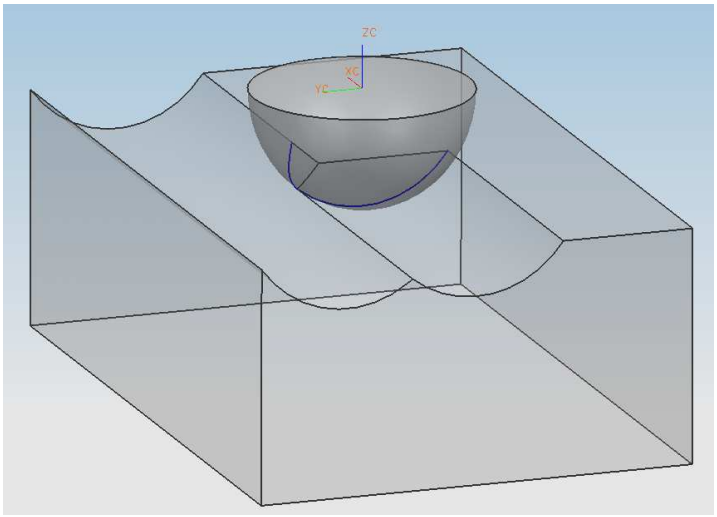

Figure 3-11 Machining of a previously machined surface

Scallop height is a measure of surface quality. Scallop height on part surface depends on radial depth of cut s and radius of the ball-end mill R_o. Scallop height h is determined from the geometric identity in Figure 3-12 and calculated by the equation below.

$$h = R_o - \sqrt{{R_o}^2 - \frac{s^2}{4}} \tag{3.24}$$

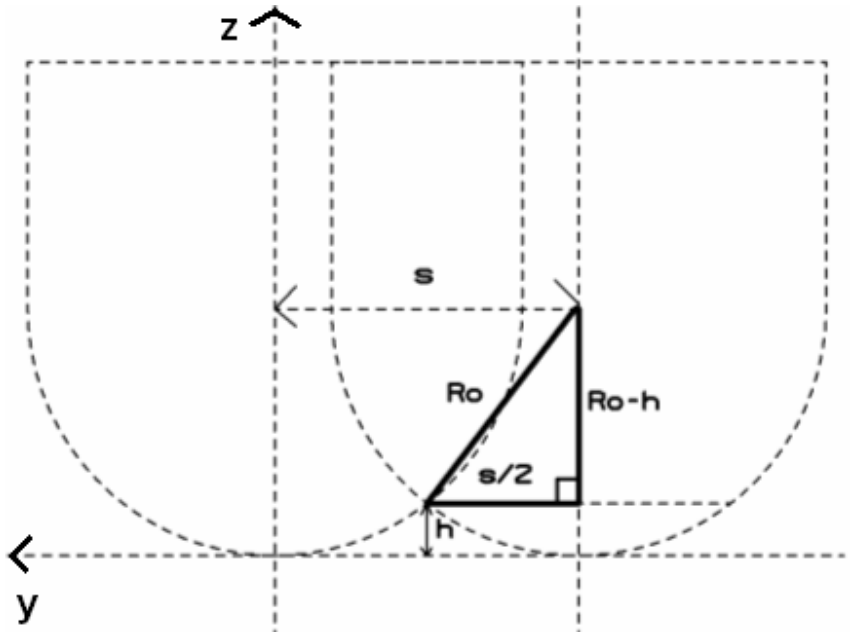

Figure 3-12 Scallop height h definition

Immersion boundaries are different for down-milling and up-milling and cases.

1. Down milling

In down milling exit angle is always π; start angle depends on radial depth of cut and axial position z when the axial position z is above the scallop height h. In this case:

$$\phi_{st}(z) = \pi - \cos^{-1}(1 - \frac{s}{R(z)}) \tag{3.25}$$

In the case when the axial position z is at a lower level than scallop height h, the cutter is in full immersion, in other words start angle is zero.

2. Up milling:

In up milling start angle is always zero; exit angle depends on radial depth of cut and axial position z when the axial position z is above the scallop height h. In this case:

$$\phi_{ex}(z) = \cos^{-1}(1 - \frac{s}{R(z)})$$

In the case when the axial position z is at a lower level than scallop height, the cutter is in fill immersion, so exit angle is equal to π.

3.5 Summary

In this chapter, the geometry of ball-end mill is presented. In ball-end mills, radius decreases as the tip point is approached. For that reason, cutting speed changes at each cross-section. Helix angle is also variable due to the changing radius. Lag angle ψ is zero at the tool tip and it reaches its maximum value of $\tan(i_o)$ at $z=R_o$. The uncut chip thickness was formulated as a function of the feed per tooth, and position of the cutting point on the ball-end mill. Engagement boundary calculations for cases of solid and previously machined surface ball-end milling were presented. These relations will be used in the following chapters for cutting force and form error modeling.

Chapter 4
5-axis Milling Geometry

4.1 Introduction

In the previous chapter, geometry of ball-end milling is explained and engagement boundaries and uncut chip thickness are defined for 3-axis milling. In this chapter, lead and tilt angles are defined; the effect of lead and tilt angles on engagement boundaries and uncut chip thickness is demonstrated.

4.2 5-axis Milling Geometry

In the 5-axis model, two coordinate systems are used: a workpiece coordinate system (WCS) XYZ and a tool coordinate system (TCS) xyz, in both of the systems the origin is taken at the ball center unlike in 3-axis milling where the origin is at the ball tip. Feed direction is taken as the X axis, Z axis is through the part's surface normal and Y axis is determined according to the right hand rule. In the tool coordinate system z axis is in the direction of the tool axis and when both lead and tilt angle are zero, x and y directions are collinear with X and Y directions, respectively (Figure 4-1).

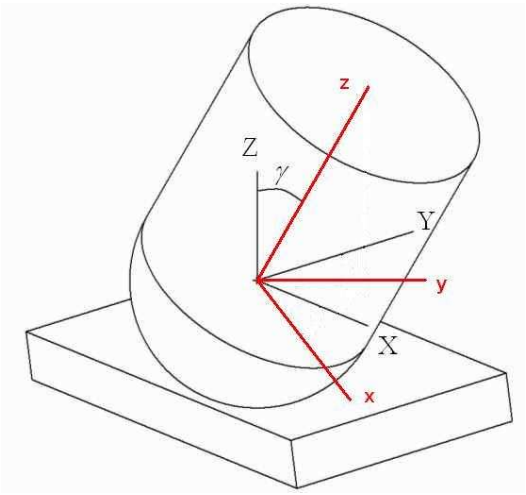

Figure 4-1 XYZ (WCS) and xyz (TCS) coordinates illustration

In 5-axis milling, there are two more additional parameters. The first one is the lead angle, angular rotation of the cutting tool about the direction perpendicular to the feed direction, and the second one is the tilt angle, angular rotation of the tool about the feed direction.

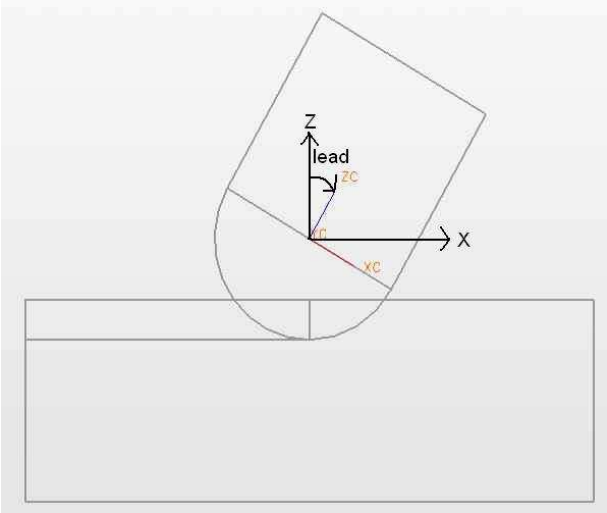

Figure 4-2 Lead angle representation

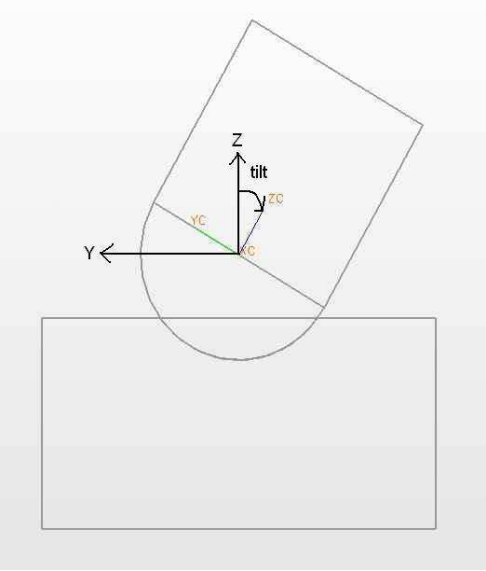

Figure 4-3 Tilt angle illustration

Any point on the cutting edge of the ball-end mill in TCS can be transformed to WCS by the transformation matrix T. T is defined as:

$$\boldsymbol{T} = \begin{bmatrix} \cos(lead) & 0 & \sin(lead) \\ \sin(tilt)\sin(lead) & \cos(tilt) & -\sin(tilt)\cos(lead) \\ -\cos(tilt)*\sin(lead) & \sin(tilt) & \cos(tilt)\cos(lead) \end{bmatrix} \tag{4.1}$$

$$\begin{bmatrix} X \\ Y \\ Z \end{bmatrix} = \boldsymbol{T} \begin{bmatrix} x \\ y \\ z \end{bmatrix} \tag{4.2}$$

For given lead and tilt angles, there is a constraint in axial depth of cut to make sure that only the ball-end part cuts the workpiece since the model considers only the cutting in the ball-end part. The allowable maximum axial depth of cut in the model is:

$$a_{\max} = R_o(1-\sin\gamma) \tag{4.3}$$

γ is the angle between Z and z-axis (Figure 4-1) and is calculated in 3 steps:

1. Define a unit vector u_1 along the tool axis in TCS

$$\boldsymbol{u}_1 = \begin{bmatrix} 0 \\ 0 \\ 1 \end{bmatrix} \tag{4.4}$$

2. Find the unit vector u_2 in XYZ corresponding to u_1.

$$\boldsymbol{u_2} = \boldsymbol{T} * \boldsymbol{u_1} = \begin{bmatrix} X_2 \\ Y_2 \\ Z_2 \end{bmatrix} \tag{4.5}$$

3. $\gamma = \cos^{-1}(Z_2)$ (4.6)

Any point in WCS can be transformed to TCS also. Inverse of the transformation matrix T is used in this conversion.

$$\begin{bmatrix} x \\ y \\ z \end{bmatrix} = \boldsymbol{T}^{-1} \begin{bmatrix} X \\ Y \\ Z \end{bmatrix} \quad (4.7)$$

4.3 Engagement Boundaries in 5-axis milling

As in 3-axis ball-end milling, engagement angles are changing along the tool axis direction, *z*. Engagement boundaries in 5-axis milling are considered by two different approaches.

4.3.1 First Approach: Analytical method

This approach uses the intersection points of geometric entities in order to calculate start and exit angles. These geometric entities are ball-end mill, top surface of the workpiece and cylinder that is created by the ball-end mill. The analytical equations of these are written in WCS and the intersection points (X_i,,Yi) are found.

1. The equation of the ball-end in WCS

First of all, the equation of the ball-end in TCS is written

$x^2 + y^2 + z^2 = {R_o}^2$, for $z \leq 0$ (4.8)

The ball-end mill equation is transformed to WCS. Transformed equation of the ball-end in WCS is:

$$X^2 + Y^2 + Z^2 = {R_o}^2, \text{ for } -R_o \le Z \le -(R_o - a) \tag{4.9}$$

2. Boundary 1 is the cylinder created by the ball-end mill, the equation of it in WCS is:

$$Y^2 + Z^2 = {R_o}^2, \text{ for } -R_o \le Z \le -(R_o - a) \tag{4.10}$$

3. Boundary 2 is the top surface of the workpiece. It's equation in WCS is:

$$Z = -(R_o - a) \tag{4.11}$$

As stated in Chapter 1, there are 8 cutting modes in 5-axis milling if 3-axis milling case is excluded. For each cutting mode a different algorithm is needed to calculate the start and exit angles. In this thesis, the mode in which lead and tilt angles are both negative will be explained to be representative.

Engagement Boundary Calculation for both lead and tilt negative case

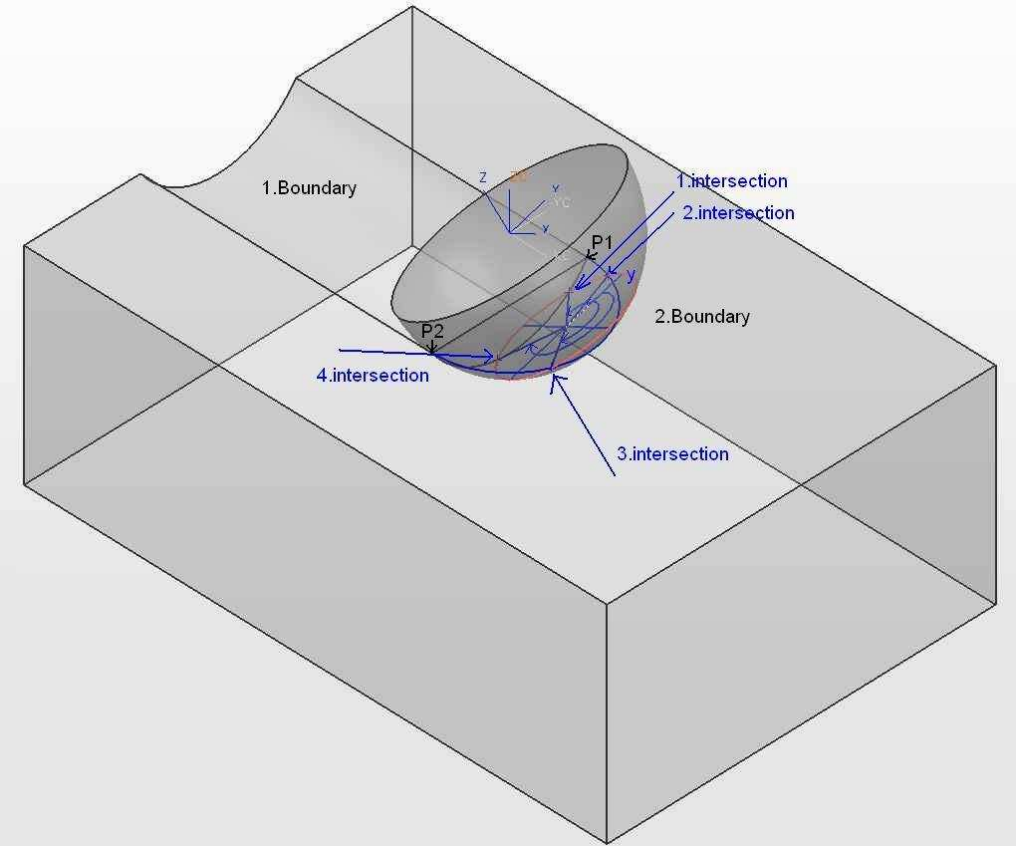

Figure 4-4 Illustration of the case when lead and tilt are both negative

There are two critical points P_1 and P_2 with coordinates in WCS (Figure 4-4):

$$P_1 = \begin{bmatrix} 0 \\ \sqrt{R_o{}^2 - (R_o - a)^2} \\ -(R_o - a) \end{bmatrix} \tag{4.12}$$

$$P_2 = \begin{bmatrix} 0 \\ -\sqrt{R_o{}^2 - (R_o - a)^2} \\ -(R_o - a) \end{bmatrix} \tag{4.13}$$

They are transformed to TCS by the inverse of the transformation matrix T to find the critical axial positions z_{lim1} and z_{lim2} as follows:

$$P_{1,TCS} = T^{-1}P_1 = \begin{bmatrix} x_1 \\ y_1 \\ z_{\lim 1} \end{bmatrix} \tag{4.14}$$

$$P_{2,TCS} = T^{-1}P_2 = \begin{bmatrix} x_2 \\ y_2 \\ z_{\lim 2} \end{bmatrix} \tag{4.15}$$

The ball-end mill is discretized into differential disks with a height of *dz*. For each differential disc, the following procedure is repeated.

In axial direction, there are 3 different zones. In the first one is z is between 0 and z_{lim1}. In this range, there is no cutting.

The second zone is between z_{lim1} and z_{lim2}. There is only one engagement region for each differential disc in this zone. The cutter first intersects with the boundary 1, the cylinder. The equation of the ball-end mill and boundary 1 are solved simultaneously and intersection point (x_1,y_1) is determined. Corresponding start angle measured from the +y direction is calculated by the atan2 function.

$$theta1 = a\tan 2(x_1, y_1) \tag{4.16}$$

The second intersection is between the cutter and the boundary 2, the top surface of the workpiece. The intersection point (x_2,y_2) is used to calculate the exit angle,theta2:

$$theta2 = a\tan 2(x_2, y_2) \tag{4.17}$$

When the z-coordinate of differential disk is less than z_{lim2}, there are 2 engaged regions. In the first engagement region, start angle is determined by the intersection of the ball-end mill and the boundary 1 which is (x_1,y_1). Likewise, exit angle is governed by the intersection of the cutter and boundary 2 that is (x_2,y_2). The tool goes out of the cut for a while and again engages with the workpiece at the start angle of the 2. engagement region where the tool intersects with the boundary 2 again at the point (x_3,y_3) . The tool stays in cut until it intersects with the boundary 1 at (x_4,y_4). Respective angles corresponding to intersection points are again determined by the atan2 function.

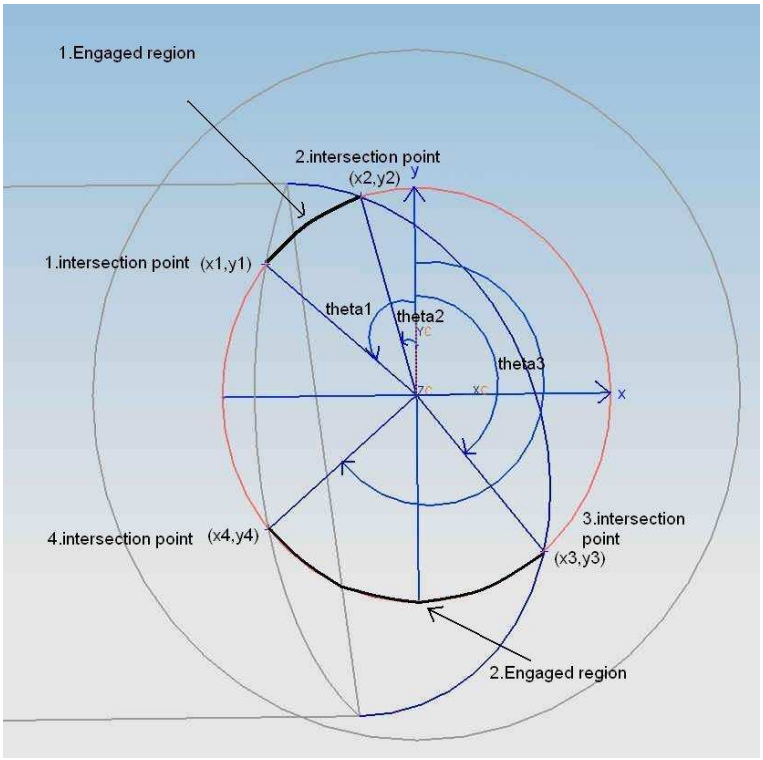

Figure 4-5 Top view along the tool axis for lead and tilt negative case; $z<z_{lim2}$ zone.

To be representative, engagement boundaries for a slot milling operation with lead and tilt angles of –15 degrees were analytically calculated and represented in the following graphs with respect to axial position z. A 12 mm. diameter ball-end mill and axial depth of cut of 3 mm are used in the calculations.

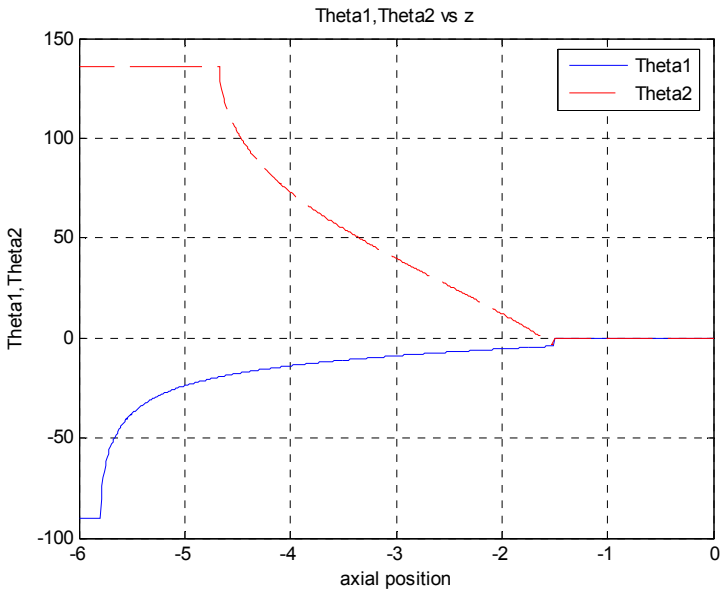

Figure 4-6 Start and exit angles in the first engagement region

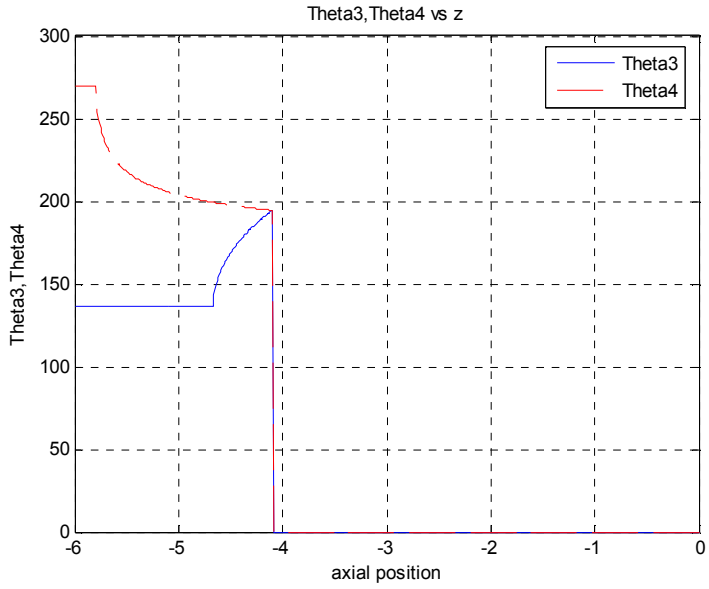

Figure 4-7 Start and exit angles in the second engagement region

This method is only applied to slot cutting, however it can be implemented for all radial depth of cut values by considering the cylinder created in the previous pass also. The disadvantage of the analytical method is that the algorithm to find start and exit angles is different for 8 different cutting modes. In the model, second method which is explained

below is preferred for engagement boundary consideration. Moreover, second method is easier to apply since it's just a modified version of engagement boundary calculation in 3-axis ball-end milling and there is no need to calculate the start and exit angles in TCS in the second method.

4.3.2 Second Method

The ball-end mill is divided into differential disc elements, having height of *dz* as in the first method and each disc is divided into differential angles. For a disc element at a height of *z*, x and y coordinates of the points on the cutting edge are found for each immersion angle ϕ as follows:

$$x = R(z)\sin\phi \tag{4.18}$$

$$y = R(z)\cos\phi \tag{4.19}$$

where *R(z)* is the radius of the ball-end mill for the particular axial position

$$R(z) = \sqrt{R_o{}^2 - z^2} \tag{4.20}$$

The coordinates of the points on the cutting edge are transformed to WCS

$$\begin{bmatrix} X \\ Y \\ Z \end{bmatrix} = \boldsymbol{T} \begin{bmatrix} x \\ y \\ z \end{bmatrix} \tag{4.21}$$

The immersion angle in the WCS can be found by atan2 function

$$\phi_{WCS}(z,\phi) = a\tan 2(X,Y) \tag{4.22}$$

In 5-axis milling, start and exit angles are calculated as in 3-axis milling. But they are written for each Z level in 5-axis milling which is in surface normal direction, not for z levels in the tool axis direction. Then a control is applied whether the point on the cutting edge is in engagement with the workpiece or not. If the point (X, Y, Z) is engaged with the workpiece it has to satisfy the following two conditions.

1. Z coordinate of the point must be between $-R_o$ and $-(R_o\text{-}a)$.

$$-R_o \le Z \le -(R_o - a)$$

2. Immersion angle at that point in WCS must be between the start and exit angles at the corresponding Z level

$$\phi_{st}(Z) \le \phi_{WCS}(z,\phi) \le \phi_{ex}(Z)$$

4.4 Uncut Chip Thickness

In 5-axis milling, uncut chip thickness at a cutting point on the cutting edge is calculated by using the immersion angle ϕ_{WCS} and K_{WCS} angle that are transformation of immersion ϕ and K angles to WCS, respectively.

$$t(\phi_j, K) = f_t \sin\phi_{jWCS} \sin K_{WCS} \tag{4.23}$$

where K_{WCS} is

$$K_{WCS} = \sin^{-1}\left(\frac{R(Z)}{R_o}\right) \tag{4.24}$$

and *R(Z)* is the radius at the Z level

$$R(Z) = \sqrt{R_o{}^2 - Z^2} \tag{4.25}$$

Chip width db, shown in Figure 3-5, which is tangent to cutting edge:

$$db = \frac{dz}{\sin K_{WCS}} \tag{4.26}$$

4.5 Summary

In this chapter, 5-axis ball-end milling geometry is presented. Two different ways to deal with the cutter-workpiece engagement was shown. While the first one is only applied to slot milling, the second one is valid for any radial depth of cut. It was shown that after making necessary transformations, 5-axis milling can be handled like 3-axis milling for determining engagement boundaries and uncut chip thickness; these relations will be used in the following chapters for cutting force and form error modeling.

Chapter 5
Force Model

5.1 Introduction

Geometry of the 5-axis milling has been presented in the previous chapters. Ball-end mill is divided into differential oblique elements and oblique cutting mechanics has been applied to find differential forces on these elements. Parameters such as shear angle, friction angle and shear stress are obtained by orthogonal to oblique transformation. Force model basically sums the elements that are engaged with the workpiece for each immersion angle and calculates resultant forces in TCS and WCS.

5.2 Force Model

In the force model, orthogonal database derived by Budak, et al. [10] for Ti6Al4V alloy is used. Shear stress on the shear plane τ_s, edge force coefficients in tangential and radial directions, chip thickness ratio r and friction angle β are given in the below table; t is uncut chip thickness in mm and α is the rake angle of the tool in degree.

$\tau_s = 613$ MPa $\beta = 19.1 + 0.29\alpha$ (rad)
$r = r_o t^a$ $r_o = 1.755 - 0.028\alpha$ $a = 0.331 - 0.0082\alpha$
$K_{te} = 24 N/mm$ $K_{re} = 43 N/mm$ $K_{ae} = 0$

Table 5-1 Orthogonal database

Normal shear angle ϕ_n and normal friction angle β_n are calculated by the equations below [1].

$$\tan(\phi_n) = \frac{r(\cos\eta / \cos i)\cos\alpha}{1 - r(\cos\eta / \cos i)\sin\alpha} \tag{5.1}$$

$$\tan(\beta_n) = \tan(\beta) * \cos\eta \tag{5.2}$$

i is the oblique angle and η is the chip flow angle. In the model, Stabler's rule [23] is used. Stabler assumes that oblique angle is equal to chip flow angle.

Cutting force coefficients K_{rc}, $K_{tc,}$ K_{ac} are calculated as follows [22]:

$$\mathrm{K_{rc}} = \frac{\tau_s}{\sin\phi_n * \cos i} * \frac{\sin(\beta_n - \alpha)}{\sqrt{\cos^2(\phi_n + \beta_n - \alpha) + \tan^2\eta * \sin^2\beta_n}}$$

$$\mathrm{K_{tc}} = \frac{\tau_s}{\sin\phi_n} * \frac{\cos(\beta_n - \alpha) + \tan i * \tan\eta * \sin\beta_n}{\sqrt{\cos^2(\phi_n + \beta_n - \alpha_n) + \tan^2\eta * \sin^2\beta_n}} \tag{5.3}$$

$$\mathrm{K_{ac}} = \frac{\tau_s}{\sin\phi_n} * \frac{\cos(\beta_n - \alpha) * \tan i - \tan\eta * \sin\beta_n}{\sqrt{\cos^2(\phi_n + \beta_n - \alpha_n) + \tan^2\eta * \sin^2\beta_n}}$$

Edge force coefficients K_{re}, $K_{te,}$ K_{ae} are directly taken from orthogonal database.

Differential cutting forces are separated into edge and shear cutting components.

$$\begin{aligned} dF_{rj}(\phi_j, K) &= K_{re} dS + K_{rc} * t(\phi_j, K) * db \\ dF_{tj}(\phi_j, K) &= K_{te} dS + K_{tc} * t(\phi_j, K) * db \\ dF_{aj}(\phi_j, K) &= K_{ae} dS + K_{ac} * t(\phi_j, K) * db \end{aligned} \tag{5.4}$$

The term dS appearing in the above differential force equations is defined in Eq. (3.12)

Differential forces in tangential, radial and axial directions are found as follows in tool coordinates system TCS [22]:

$$\begin{bmatrix} dF_{xj}(\phi_j, K) \\ dF_{yj}(\phi_j, K) \\ dF_{zj}(\phi_j, K) \end{bmatrix} = \boldsymbol{T}_{xyz} \begin{bmatrix} dF_{rj}(\phi_j, z) \\ dF_{tj}(\phi_j, z) \\ dF_{aj}(\phi_j, z) \end{bmatrix} \tag{5.5}$$

$$\boldsymbol{T}_{xyz} = \begin{bmatrix} -\sin K * \sin\phi_j & -\cos\phi_j & -\cos K * \sin\phi_j \\ -\sin K * \cos\phi_j & \sin\phi_j & -\cos K * \cos\phi_j \\ \cos K & 0 & -\sin K \end{bmatrix} \tag{5.6}$$

Immersion angle ϕ_j and K angle is defined in Figure 3-2.

Cutting forces in TCS are calculated by summing the differential forces acting on the oblique elements engaged with the workpiece for each immersion angle.

$$\begin{aligned} F_x(\phi) &= \sum dF_{xj}(\phi_j, K) \\ F_y(\phi) &= \sum dF_{yj}(\phi_j, K) \\ F_z(\phi) &= \sum dF_{zj}(\phi_j, K) \end{aligned} \tag{5.7}$$

Cutting forces are then transformed to WCS by using the transformation matrix T:

$$\begin{bmatrix} F_X(\phi) \\ F_Y(\phi) \\ F_Z(\phi) \end{bmatrix} = \boldsymbol{T} \begin{bmatrix} F_x(\phi) \\ F_y(\phi) \\ F_z(\phi) \end{bmatrix} \tag{5.8}$$

5.3 Summary

In this chapter, force modeling of ball-end milling is presented. Cutting and edge force coefficient calculations are determined using mechanics of milling method. In this method, orthogonal to oblique transformation is used for the calculation of cutting force coefficients. The procedure is demonstrated on Ti_6Al_4V alloy database. Expressions for forces on differential oblique elements are demonstrated together with the necessary transformations to find forces in TCS and WCS. Finally, differential forces are summed to calculate the cutting forces in xyz and XYZ directions for each immersion angle.

Chapter 6
Form Error

6.1 Introduction

Form error is a measure of quality of a finished product. The usual procedure to maintain the tolerance integrity is through using conservative cutting parameters such as feed and depth of cuts and/or measuring the form errors and offsetting the tool path. These results in decreased productivity due to the conservative cutting parameters and several scrap parts until a proper offsets identified. However, if the form error is modeled for a cutting process before machining, the part can be machined right at the first try by offsetting the tool path by the error amount predicted. This is the motivation for modeling the form error in this thesis.

6.2 Form Error Model

For predicting the form error in a cutting operation, tool and workpiece are structurally modeled and cutting forces are applied on these structural models to determine deformations. Form error is the relative deformation between the tool and workpiece . Since the form error presented in this thesis is a general model, and the structure of the workpiece in 5-axis milling is application specific, only the deformation in the tool is considered. If necessary, the part deformations can be determined through the Finite Element Analysis.

Ball-end mill can be modeled as a cylindrical cantilever beam as shown in Figure 6-1. Cutting forces on the ball-end mill in x and y directions are transversal loads, whereas the cutting force in axial z direction is an axial force.

There is a surface generation point at each engaged differential disk. If the process is up-milling, at surface generation point immersion angle is equal to 0. However, if it’s down-

milling surface is generated when immersion angle is equal to π. There are two geometric variables in calculation of the tool deformations based on the beam model [19]. v_k and v_m ,which are the distances of the surface generation point and the force application point from the connection point of the tool and the tool holder, respectively (Figure 6-1). Forces in x and y directions are assumed to be acting at the average axial position of the surface generation points.

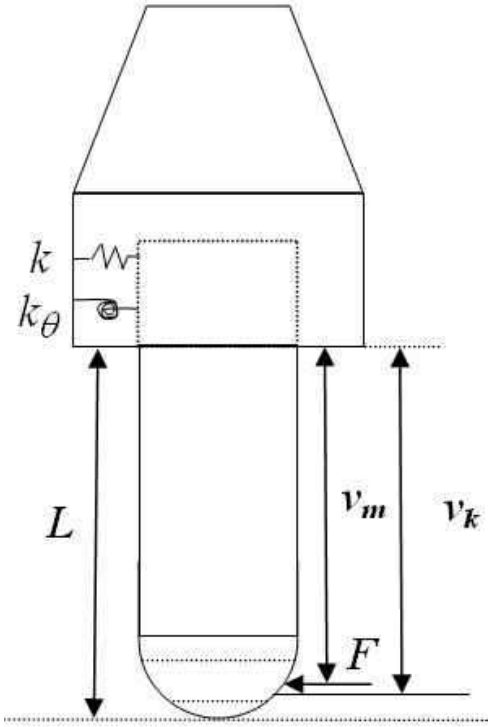

Figure 6-1 Structural Model of the ball-end mill in x and y directions

The tool holder is assumed to be rigid and tool is connected to the tool holder by linear spring k, and torsion spring $k\theta$ in x and y directions. k and $k\theta$ are identified by applying loads on the tool and measuring the deformation of the tool at two different positions.

The mentioned identification procedure was applied the tool which is used in the 5-axis cutting experiments for four different force levels. The results of these studies are tabulated in the below table.

F(N)	k(N/mm)	k_θ (N.mm/rad)
250	6250	$1.624*10^7$
500	6410	$1.671*10^7$
750	6356	$1.666*10^7$
1000	6211	$1{,}663*10^7$

Table 6-1 Transversal forces vs. k and k_θ

Since the cutting forces generally encountered are below 1000 N, an average value of 6306 N/mm for k and $1.656*10^7$ N.mm/rad for k_θ can be used in the deformation model for the corresponding tool. The tool is clamped to the tool holder by a shrink fit machine.

Deformation in x and y directions are found by the following formulas [19]. If v_m is greater than v_k, in other words if force application point is at a lower level than surface generation point:

$$\delta_p(z) = \frac{F_p {v_k}^2}{6EI}(3v_m - v_k) + \frac{F_p}{k} + \frac{F_p v_m v_k}{k_\theta} \quad p = x, y \tag{6.1}$$

In the other case where force application point is at a higher level than surface generation point,

$$\delta_p(z) = \frac{F_p {v_m}^2}{6EI}(3v_k - v_m) + \frac{F_p}{k} + \frac{F_p v_m v_k}{k_\theta} \quad p = x, y \tag{6.2}$$

Deformation in z direction can be modeled as an axial deformation of a cylindrical beam element as:

$$\delta_z(z) = \frac{F_z * L}{EA} \tag{6.3}$$

where E is Young's modulus, I is the area moment of inertia of the cutter and L is the overhang.

Deformations in TCS are transformed to WCS by the transformation T:

$$\begin{bmatrix} \delta_X(Z) \\ \delta_Y(Z) \\ \delta_Z(Z) \end{bmatrix} = \boldsymbol{T} \begin{bmatrix} \delta_x(Z) \\ \delta_y(Z) \\ \delta_z(Z) \end{bmatrix} \tag{6.4}$$

Deformation in the surface normal direction is calculated by the following relation:

$$\delta_n(Z) = \delta_Y(Z)\sin K_{WCS} + \delta_Z(Z)\cos K_{WCS} \tag{6.5}$$

6.3 Summary

Tool deformation is modeled in this chapter. Only the deformation of the tool is considered in this thesis since workpiece is a process specific variable. The tool is modeled as a cantilever beam and beam equations are used to model the deformation of the tool. Deformations in TCS are calculated and they are transformed to WCS. Finally, calculation of deformation in the surface normal direction is demonstrated.

Chapter 7
Simulations and Experimental Results

7.1 Experiments

5-axis milling tests were conducted on a Deckel Maho DMU 50 Evolution Machining Center. A Kistler table type dynamometer was used to measure the forces during milling (Figure 7-1). Cutting conditions for the cutting tests are given in Table 7-1. Nine cutting tests are performed where lead and tilt angles were changed between -15, +15 deg. Corresponding lead and tilt angles for the tests are tabulated in Table 7-2.

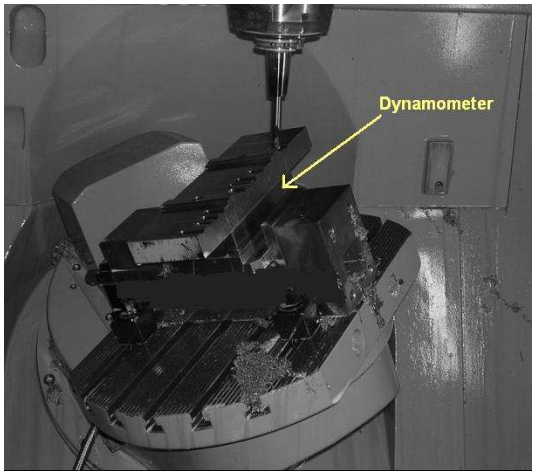

Figure 7-1 Test setup

Workpiece	Ti_6Al_4V
Tool	12 mm diameter, 1 tooth carbide ball-end mill 30 deg. helix angle
Cutting Type	Slot Cutting
Axial depth of cut	3 mm
Feed	0.1 mm/(rev*tooth)
Cutting Speed	269 rpm

Table 7-1 Cutting conditions

Test No	lead	tilt
	(deg)	(deg)
1	15	15
2	0	15
3	-15	15
4	15	0
5	0	0
6	-15	0
7	15	-15
8	0	-15
9	-15	-15

Table 7-2 Lead and tilt angles applied in the tests

7.2 Comparison of Simulations and Experiments

Cutting conditions of these 9 tests with corresponding lead and tilt angles were inserted to the 5-axis force model and cutting forces were simulated for one revolution of the cutting tool. Simulated and measured cutting forces are compared below.

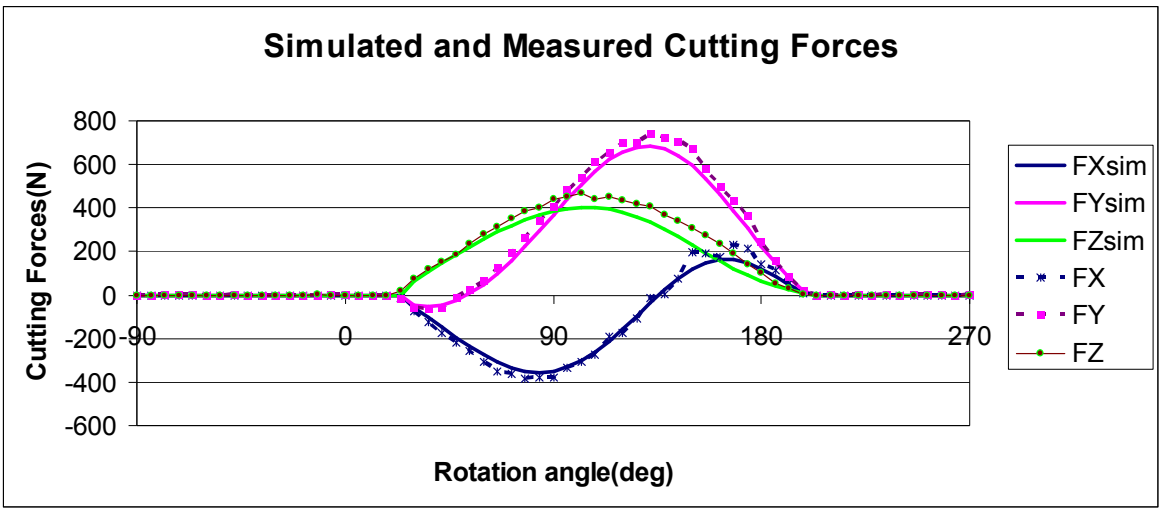

Figure 7-2 Test 1: lead 15 deg & tilt 15 deg

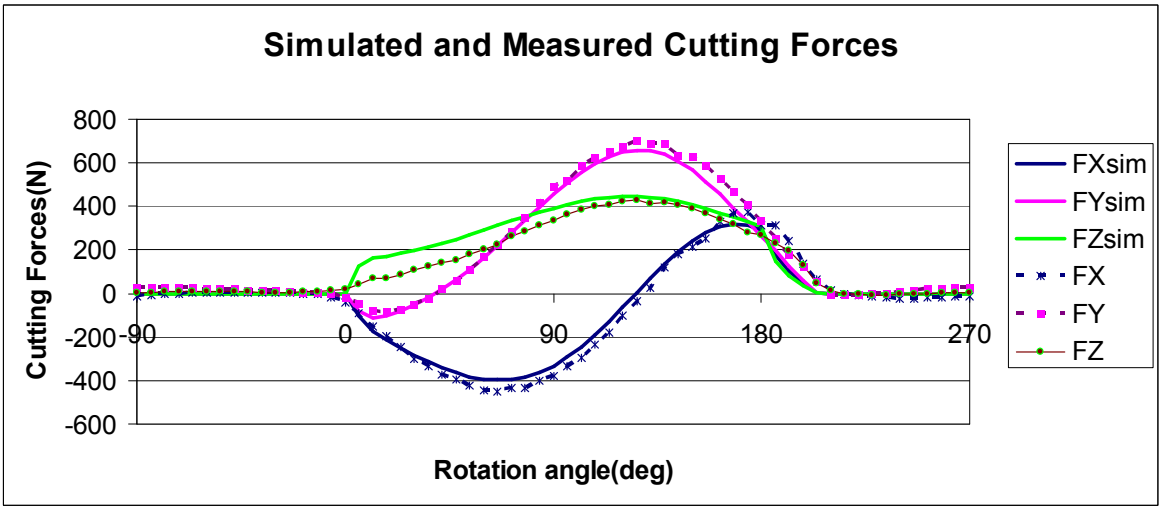

Figure 7-3 Test 2: tilt 15 deg

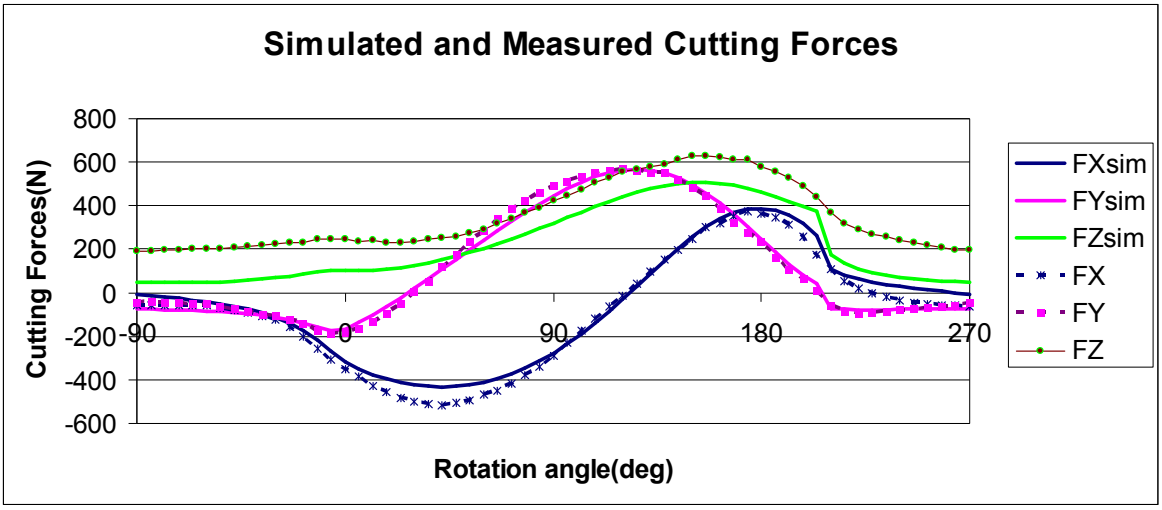

Figure 7-4 Test 3: lead -15 deg & tilt 15 deg

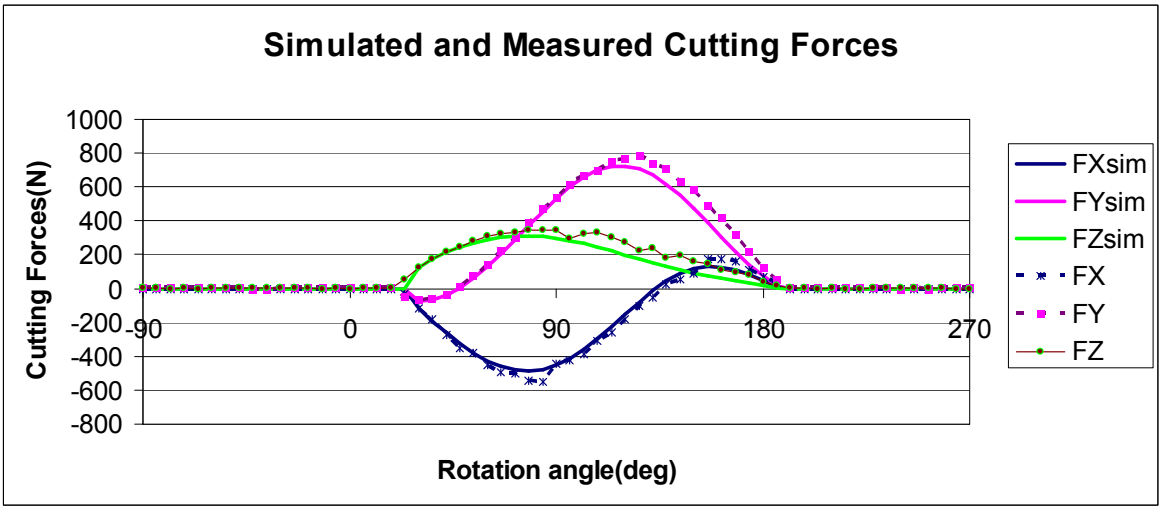

Figure 7-5 Test 4: lead 15 deg

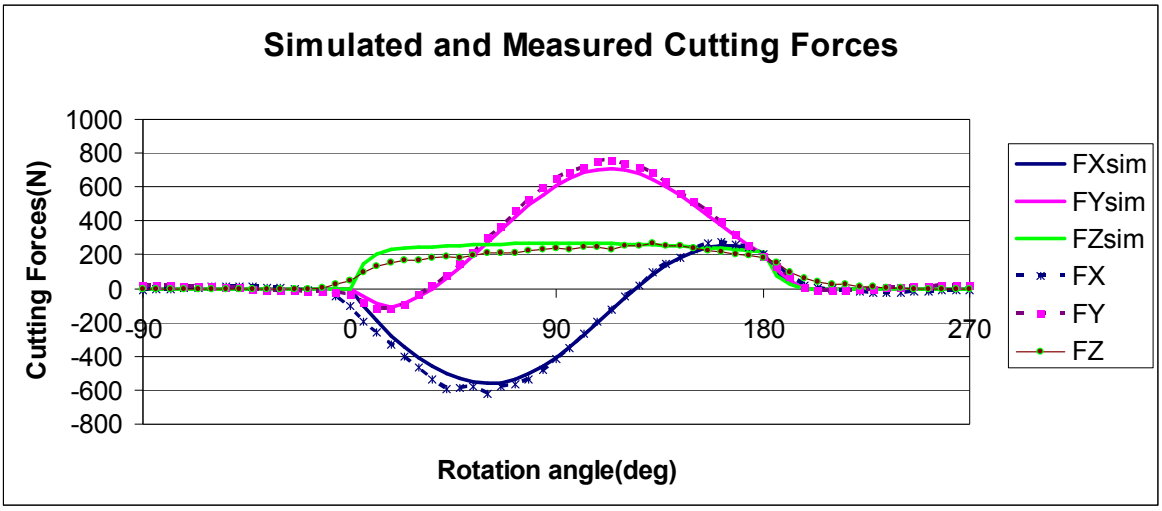

Figure 7-6 Test 5: lead 0 deg & tilt 0 deg

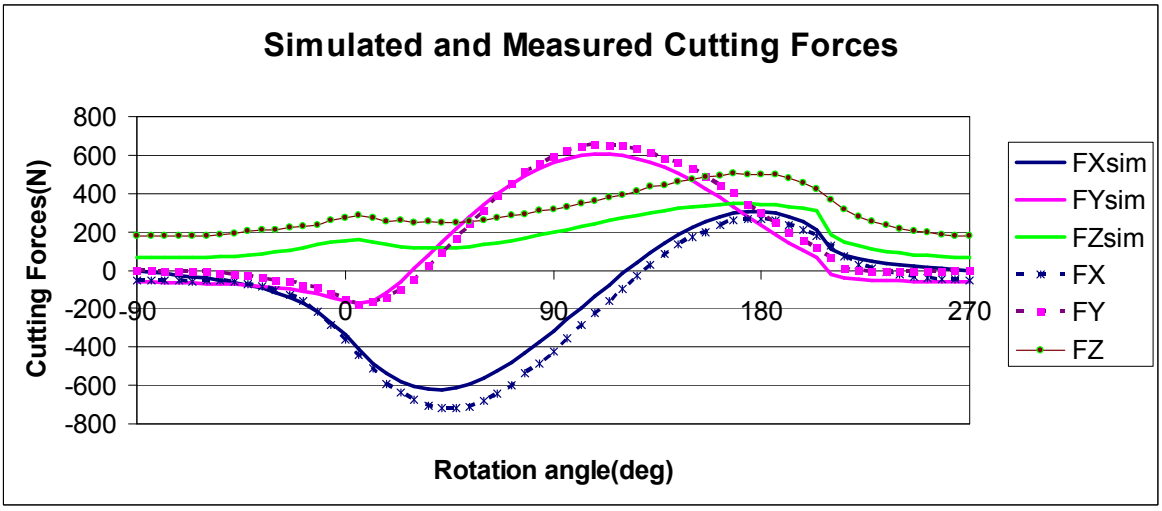

Figure 7-7 Test 6: lead -15 deg

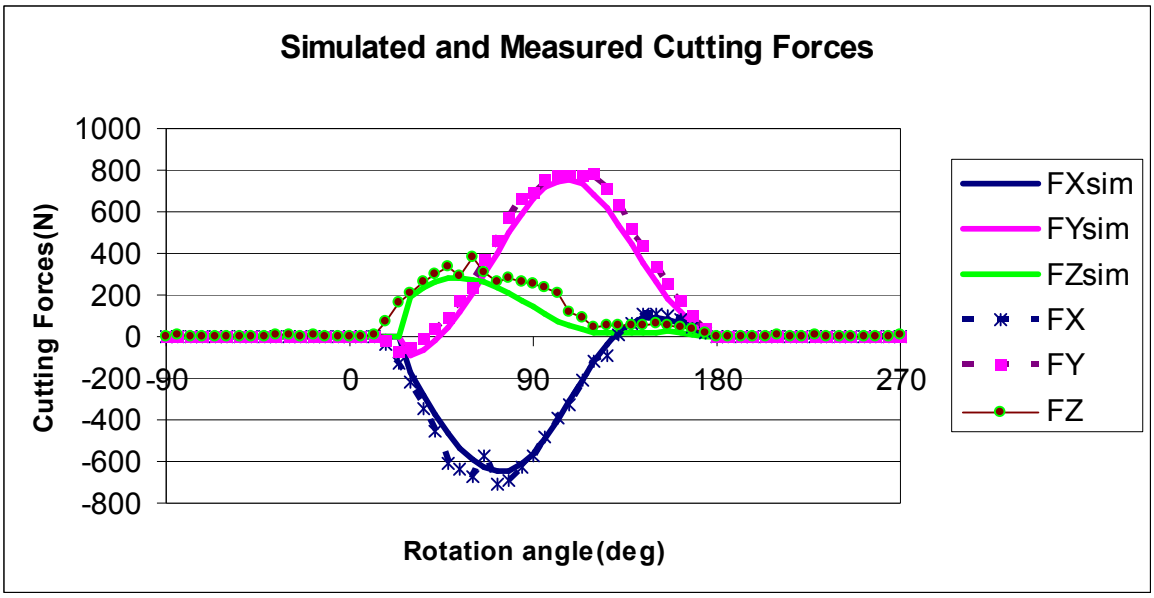

Figure 7-8 Test 7: lead 15 deg & tilt -15 deg

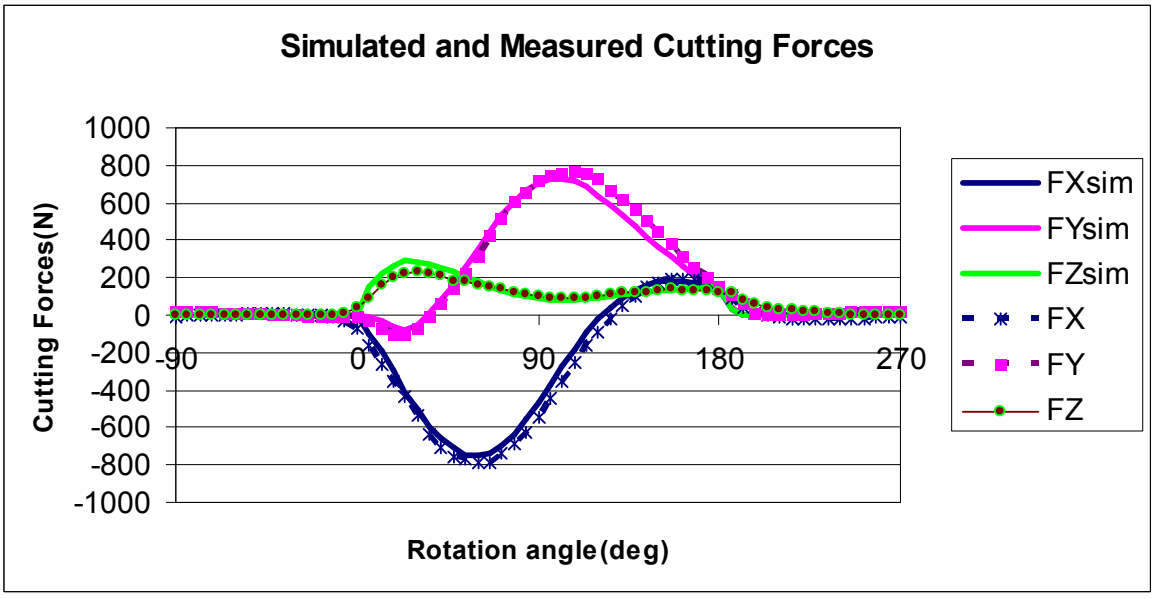

Figure 7-9 Test 8: tilt -15 deg

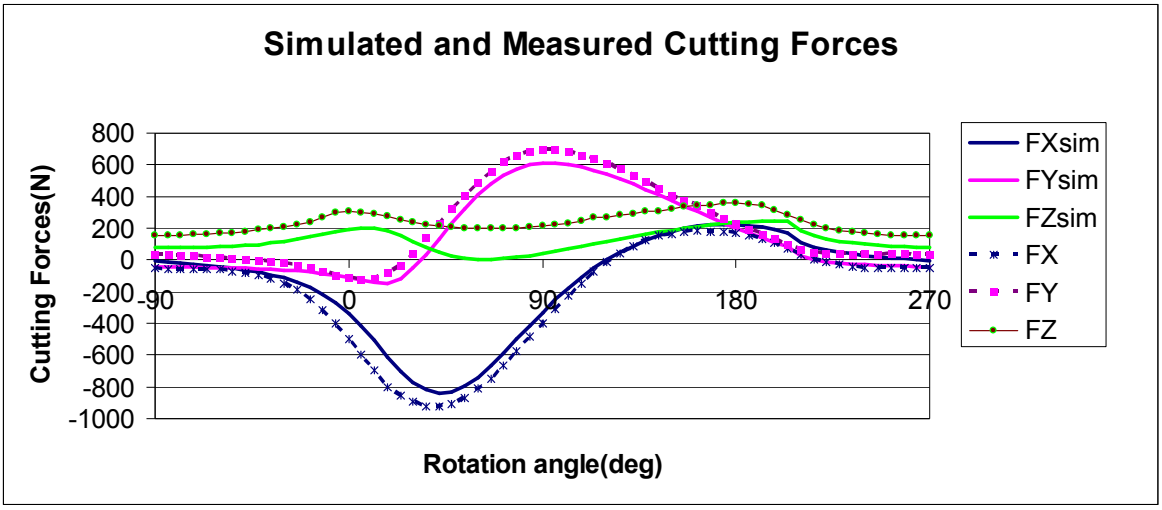

Figure 7-10 Test 9: lead -15 deg & tilt -15 deg

The waveform and magnitudes of the simulated forces are in reasonably good agreement with the experimental data except the cases where lead angle is negative. When lead angle is negative, it is observed that simulation is underestimating the cutting forces. The reason for this situation is that the tip of the ball-end mill is in contact with the workpiece and feed vector has a nonzero component in the tool axis direction. Hence, the tool tip is trying to enter to the workpiece .This phenomena can not be explained by cutting mechanism since cutting speed is zero at the tool tip. Since there is a contact between the tool and workpiece at the tool tip, a certain contact pressure occurs. This pressure needs to be modeled for accurate prediction of forces in 5-axis milling. Nevertheless, the model's predictions for forces in 5-axis milling can be used as a reference keeping in mind the underestimation when lead angle is negative.

For nine tests, max values of forces measured and predicted by the simulations in Y and Z directions are tabulated in Table 7-3. X direction is not taken into consideration, since it doesn't have effect on the surface generation mechanism. Combinations of lead and tilt angles resulting in the minimum force are shown in green and the combinations resulting in the maximum force are highlighted with red.

lead	tilt	FY(max)	FZ(max)	FYsim(max)	FZsim(max)
(deg)	(deg)	(N)	(N)	(N)	(N)
15	15	740	469	684	404
0	15	700	430	659	446
-15	15	570	628	567	507
15	0	785	347	723	310
0	0	756	268	708	268
-15	0	653	505	604	346
15	-15	778	379	753	283
0	-15	772	227	731	294
-15	-15	696	359	731	246

Table 7-3 Maximum Force Values in Y and Z directions; Experimental and simulated

7.3 Optimum combination of lead and tilt angles

There can be different objectives for finding the optimum combination of lead and tilt angles. Two objectives are presented in this thesis. The first objective is force minimization and the second one is form error minimization.

7.3.1 Force Minimization

In the experiments, the force in Y direction is minimum when lead angle and tilt angle combination of (-15, 15) deg is applied. Simulation also predicts that minimum force in Y direction is at (-15, 15) deg combination. At (-15, 15) deg combination, however, force in Z direction is maximum both in the experiment and in the simulation. The force in Z direction is minimum at (0,-15) deg combination in the experiments and it's minimum at (-15,-15) combination. This difference is due to the underestimation behaviour in the simulation when lead angle is negative. At the combinations where the force in Z direction is minimum, force in Y directions are close to maximum in both experiments and in the simulations. An important result from these comparisons is that the response of forces in Y and Z directions to lead and tilt angles are quite contradictory. Unless there is a specific objective to minimize the forces in one direction or to minimize the resultant forces, it's not

possible to decide on an optimum lead and tilt angle combination by just checking the magnitudes of the forces.

7.3.2 Form Error Minimization

As presented in Chapter 6, tool deformation in surface normal direction is a function of forces in Y and Z directions, so their contradictory behavior is combined in calculation of tool deformation. Therefore, form error minimization is suitable to be an objective function for finding optimum lead and tilt angle combination.

Deformation model were run for the same conditions as in Table 7-1 and Table 7-2. The parameters related to the cutting tool are:

L	65 mm
Young's Modulus,E	200 GPa
k	6306 N/mm
$k\theta$	$1.656*10^7$ N.mm/rad

Table 7-4 Tool parameters

As a result of the simulations, it is observed that minimum tool deformation in surface normal direction occurs at (0, 15) deg combination and it is maximum at (15, 15) deg combination. So, using the lead and tilt angle combination of (0, 15) deg is preferable for the given cutting conditions. The tool deformation in surface normal direction with respect to Z coordinates of the surface generation points for these two cases are graphed below:

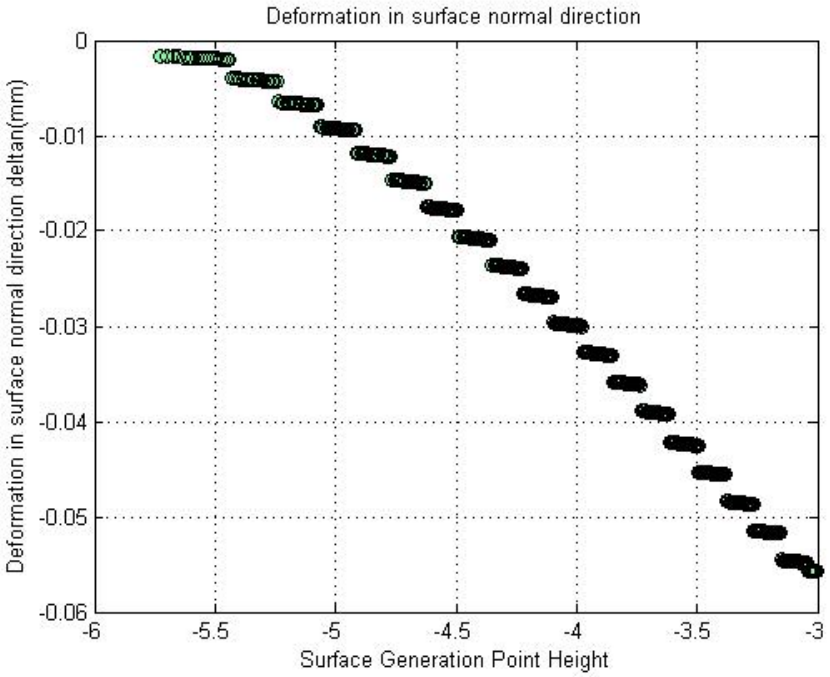

Figure 7-11 Deformations for lead 0 deg & tilt 15 deg case

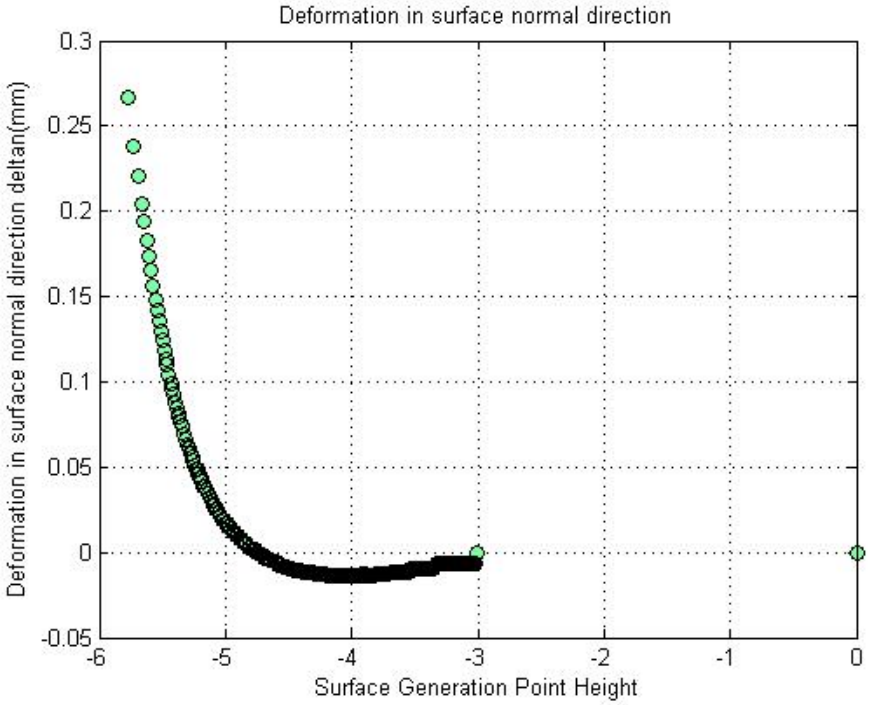

Figure 7-12 Deformations for lead 15 deg & tilt 15 deg case

Chapter 8
Conclusions

The modeling of cutting forces and form error in 5-axis milling is presented in this thesis. The formulations for the geometry and the forces are given in detail by demonstrating the effects of lead ant tilt angles. Simulated and measured milling forces are compared and it is demonstrated that the model can predict the 5-axis milling forces with reasonable accuracy. The effects of the lead and tilt angles on the forces and form error, and preferred 5-axis milling conditions are determined for minimizing the form error in surface normal direction.

8.1 Future Research Directions

The form error predictions of the model are to be compared and verified by experimental results.

The model currently takes cutting parameters such as axial, radial depths of cut, lead and tilt angles by user input. By another work going parallel with this thesis, from an APT code of a part the stated parameters will be extracted. This will increase the industrial applicability of the thesis.

The encountered underestimation problem in cutting forces when lead angle is negative needs to be modeled in order to predict cutting forces more accurately.

Dynamics of 5-axis ball-end milling are to be modeled to find stable depth of cuts in order to have a chatter free cutting operation and avoid possible chatter marks on the surface.

Bibliography

1. Armarego, E.J.A. and Brown, R.H., 1969, "The Machining of Metals", Prentice-Hall

2. Merchant M. Eugene, 'Basic Mechanics of the Metal Cutting Process'.

3. Shatla, M., and Altan, T., 2000, 'Analytical Modeling of Drilling and Ball-End Milling', Journal of Materials Processing Technology, 98, 125-133

4. W. Lee, C. Lin, 'High Temperature deformation behavior of Ti6Al4V alloy evaluated by high strain-rate compression tests' , Journal of Materials Processing Technology, 75,1998, 127-136

5. T. Obikawa, E. Usui, 'Computational Machining of titanium alloy, finite element modeling and a few results' , Trans. ASME 118 (1996) , 208-215

6. A. Moufki, A. Devillez, D. Dudzinski, A. Molinari, 'Thermomechanical modelling of oblique cutting and experimental validation' , International Journal of Machine Tools and Manufacture, 44, 2004, 947-954

7. Gradisek, J. , Kalveram M. , Weinert, K. , 'Mechanistic Identification of Specific Force Coefficients for a General End Mill' , International Journal of Machine Tools and Manufacture, 44, 2004, 401-414

8. Yucesan, G., and Altintas, Y., 1996, 'Prediction of Ball-end Milling Forces', Journal of Engineering for Industry, Vol.118, pp 95-103.

9. Lazoglu, I., 2003, 'Sculpture Surface Machining: A Generalized Model of Ball-End Milling Force System', Int. J. Mach. Tools Manufact., 43, 453-462.

10. Budak, E., Altintas, Y., and Armarego, E. J. A., 1996, 'Prediction of Milling Force Coefficients from Orthogonal Cutting Data' ASME Journal of Engineering for Industry.

11. Lee, P. and Altintas, Y., 1996, ' Prediction of Ball-End Milling Forces From Orthogonal Cutting Data,' Int. J. Mach. Tools Manufact., 36, pp 1059-1072.

12. Yang, M., and Park, H., 1991,'The Prediction of Cutting Force in Ball-End Milling', Int. J. Mach. Tools Manufact., 31(1): 45-54.

13. Sadeghi, M. H., Haghighat, H. and Elbestawi, M. A, 2003, 'A Solid Modeler based Ball-End Milling Process Simulation', Int. J. Adv. Manuf. Technol, 22, 775-785.

14. Tai, C., Fuh, K.,1995, ' The Prediction of Cutting Forces in the Ball-End Milling Process', Journal of Materials Processing Technology, 54, 286-301.

15. Lazoglu, I., and Liang, S. Y., 2000, 'Modeling of Ball-End Milling Forces with Cutter Axis Inclination', Journal of Manufacturing Science and Engineering, Vol.122.

16. Fussell, B.K., Jerard, R. B., and Hemmet, J. G., 2003, ' Modeling of Cutting Geometry and Forces for 5-axis Sculptured Surface Machining', Computer Aided Design, 35, 333-346.

17. Clayton, P. A., El-Wardany, T., Elbestawi, M. A., and Viens D., 2000, 'A Mechanistic Force Model of the 5-Axis Milling Process', Proceedings of the ASME Manufacturing Engineering Division, Vol.11.

18. Zhu, R. ,Kapoor, S. G. , DeVor, R. E., 2001, ' Mechanistic Modeling of the Ball-end Milling Process for Multi-Axis Machining of Free-Form Surfaces' , Journal of Manufacturing Science and Engineering, Vol.123, 369-379

19. Budak, E. and Altıntaş, Y. , ‘ Peripheral Milling Conditions for Improved Dimensional Accuracy’ , International Journal of Machine Tools and Manufacture, Vol. 34, No:7, 1994, 907-918.

20. Kim, G. M. , Kim, B. H. and Chu, C. N. , ’Estimation of Cutter Deflection and Form Error in Ball-end Milling Processes’, International Journal of Machine Tools and Manufacture, Vol. 43, 2003, 917-924.

21. Ryu, S. H. , Lee, H. S. , Chu, C. N. , ‘ The form error prediction in side wall machining considering tool deflection’ , International Journal of Machine Tools and Manufacture, Vol. 43, 2003, 1405-1411.

22. Altintas, Y., ‘Manufacturing Automation Metal Cutting Mechanics, Machine Tool Vibrations, and CNC Design’, Cambridge University Press 2000.

23. Stabler, G. V. , ‘The Chip Flow Law and Its Consequences’, Advances in Machine Tool Design and Research, pages 243-251, 1964

24. http://www.mathworks.com/